Optik 124 (2013) 3017–3021

Contents lists available at SciVerse ScienceDirect

Optik

journal homepage: www.elsevier.de/ijleo

Target detection using difference measured function based matched filter for hyperspectral imagery☆

Zhenwei Shi[a,b,c,*], Shuo Yang[a], Zhiguo Jiang[a,b]

[a] Image Processing Center, School of Astronautics, Beihang University, Beijing 100191, PR China
[b] Beijing Key Laboratory of Digital Media, Beihang University, Beijing 100191, PR China
[c] State Key Laboratory of Virtual Reality Technology and Systems, Beihang University, Beijing 100191, PR China

ARTICLE INFO

Article history:
Received 11 May 2012
Accepted 10 September 2012

Keywords:
Hyperspectral image processing
Target detection
Difference measured function

ABSTRACT

Automatic target detection is a research focus in hyperspectral image processing field. Algorithms such as the matched filter (MF) and the adaptive coherence/cosine estimator (ACE) directly use the prior knowledge of target spectral signatures to detect targets. In this paper, we propose a difference measured function based matched filter (DFMF), which could include the famous algorithm MF as a special case. The DFMF uses a new measured function to build an objective function, and utilizes the gradient descent method to find an optimal projection vector. After finding the optimal projection vector, the interesting targets can be detected in the projection space. The experimental results demonstrate the proposed algorithm could detect interesting targets effectively and performs better than some other experimental algorithms.

1. Introduction

The hyperspectral image with two spatial dimensions and one spectral dimension is referred to "data cube" [1]. A prominent feature of the hyperspectral image is the high spectral resolution. The hyperspectral imaging sensor provides each pixel a nearly continuous spectrum which usually has dozens of or hundreds of narrow bands, and the width of each band is usually about 10 nm [2,3]. Utilizing the spectral information, targets of interest can be detected effectively. Due to the important applications both in the military and the civilian fields, the automatic target detection has become a research focus in the hyperspectral image processing field.

Several target detection algorithms for hyperspectral images have been developed. The matched filter (MF) [1,4,5] and the adaptive coherence/cosine estimator (ACE) [1,6–9] are two famous algorithms. Both the MF and the ACE have geometric interpretations. If we use the whitening transformation, which can make the components of spectra be uncorrelated and their variances equal unity, the output of the MF can be seen as the projection of the whitened test pixel's spectrum to the whitened target signature, and the output of the ACE can be seen as the cosine square of the angle between the whitened test pixel's spectrum and the whitened target signature [1,10]. Thus, both the MF and the ACE measure the similarity of the test pixel's spectrum and the target signature in the whitened space, but in different ways. Another famous and widely used target detection algorithm is the constrained energy minimization (CEM) [11–13] detector. The formulations of the MF and the CEM are very similar. In fact, if we do a mean removing preprocessing, the CEM becomes the MF [1].

In this paper, we propose a difference measured function based matched filter (DFMF) which uses a new measurement, and can include the MF as a special case. The algorithm finds an optimal projection vector through solving a constrained optimization problem. Then, we project the whitened test pixels' spectra to the optimal projection vector, and detect interesting targets in the projection space.

The following paper is organized as follows. In Section 2, we give a brief introduction to the MF and the ACE. Section 3 proposes the new algorithm, and Section 4 proofs the stability of the proposed algorithm. In Section 5, some experimental results and analyses are given. Some conclusions are drawn in Section 6.

2. A brief introduction to the MF and the ACE

The spectrum of a K-band pixel can be represented in a vector form as $\mathbf{x} = [x_1, \ldots, x_K]^T$, where T denotes matrix transpose. The

☆ The work was supported by the National Natural Science Foundation of China under the grants 61273245, 60975003 and 91120301, the 973 Program under the grant no. 2010CB327904, the open funding project of State Key Laboratory of Virtual Reality Technology and Systems, Beihang University (grant no. BUAA-VR-12KF-07), the Program for New Century Excellent Talents in University of Ministry of Education of China under the grant no. NCET-11-0775, and the Beijing Natural Science Foundation (Non-negative Component Analysis for Hyperspectral Imagery Unmixing) under the grant no. 4112036.

* Corresponding author at: Image Processing Center, School of Astronautics, Beihang University, Beijing 100191, PR China. Tel.: +86 10 823 39 520; fax: +86 10 823 38 798.
E-mail address: shizhenwei@buaa.edu.cn (Z. Shi).

0030-4026/$ – see front matter © 2012 Elsevier GmbH. All rights reserved.
http://dx.doi.org/10.1016/j.ijleo.2012.09.003

spectra of an N-pixel hyperspectral image can be arranged in a matrix form as $\mathbf{X}=[\mathbf{x}(1), \ldots, \mathbf{x}(N)]$, where the size of $\mathbf{X}$ is $K \times N$. A K-dimensional vector $\mathbf{d}=[d_1, \ldots, d_K]^T$ is used to represent the spectral signature of the interesting target, and $\mathbf{d}$ can be obtained from the spectral library.

For a pixel's spectrum $\mathbf{x}$, the output values of the famous MF and ACE are [1]:

$$y_{MF} = D_{MF}(\mathbf{x}) = \frac{(\mathbf{x}-\boldsymbol{\mu})^T \boldsymbol{\Gamma}^{-1}(\mathbf{d}-\boldsymbol{\mu})}{(\mathbf{d}-\boldsymbol{\mu})^T \boldsymbol{\Gamma}^{-1}(\mathbf{d}-\boldsymbol{\mu})} \tag{1}$$

$$y_{ACE} = D_{ACE}(\mathbf{x}) = \frac{[(\mathbf{d}-\boldsymbol{\mu})^T \boldsymbol{\Gamma}^{-1}(\mathbf{x}-\boldsymbol{\mu})]^2}{(\mathbf{d}-\boldsymbol{\mu})^T \boldsymbol{\Gamma}^{-1}(\mathbf{d}-\boldsymbol{\mu})(\mathbf{x}-\boldsymbol{\mu})^T \boldsymbol{\Gamma}^{-1}(\mathbf{x}-\boldsymbol{\mu})} \tag{2}$$

where $\boldsymbol{\mu}=E\{\mathbf{x}\}$ is the mean spectrum of the hyperspectral image, and $\boldsymbol{\Gamma}=E\{(\mathbf{x}-\boldsymbol{\mu})(\mathbf{x}-\boldsymbol{\mu})^T\}$ is the covariance matrix. Usually, $D_{MF}(\mathbf{x})$ or $D_{ACE}(\mathbf{x})$ is compared to a threshold η. If $D_{MF}(\mathbf{x})>\eta$ or $D_{ACE}(\mathbf{x})>\eta$, $\mathbf{x}$ is determined as a target pixel; otherwise, it is determined as background. If we use $\tilde{\mathbf{x}}$ to denote $\boldsymbol{\Gamma}^{-1/2}(\mathbf{x}-\boldsymbol{\mu})$ and $\tilde{\mathbf{d}}$ to denote $\boldsymbol{\Gamma}^{-1/2}(\mathbf{d}-\boldsymbol{\mu})$, y_{MF} and y_{ACE} can be rewritten as [1]:

$$y_{MF} = D_{MF}(\mathbf{x}) = \frac{\tilde{\mathbf{d}}^T \tilde{\mathbf{x}}}{\tilde{\mathbf{d}}^T \tilde{\mathbf{d}}} \tag{3}$$

$$y_{ACE} = D_{ACE}(\mathbf{x}) = \frac{(\tilde{\mathbf{d}}^T \tilde{\mathbf{x}})^2}{\|\tilde{\mathbf{d}}\|^2 \|\tilde{\mathbf{x}}\|^2} = \cos^2\theta \tag{4}$$

where θ is the angle between $\tilde{\mathbf{d}}$ and $\tilde{\mathbf{x}}$. $\boldsymbol{\Gamma}^{-1/2}(\mathbf{x}-\boldsymbol{\mu})$ and $\boldsymbol{\Gamma}^{-1/2}(\mathbf{d}-\boldsymbol{\mu})$ can be seen as the whitening processing. After the whitening processing, the covariance of the whitened $\tilde{\mathbf{x}}$ is $\mathbf{I}$, which means the whitened data's components are uncorrelated and their variances equal unity [1,10]. Note that $\tilde{\mathbf{d}}^T \tilde{\mathbf{d}}$ is a constant, and has no influence to the detection result. From (3) and (4), it can be seen that the output of MF is the projection of $\tilde{\mathbf{x}}$ to $\tilde{\mathbf{d}}$, and the output of ACE is the cosine square of the angle between $\tilde{\mathbf{x}}$ to $\tilde{\mathbf{d}}$ [1]. In fact, the MF and the ACE directly use the similarity of $\tilde{\mathbf{d}}$ and $\tilde{\mathbf{x}}$ in the whitened space to determine whether $\tilde{\mathbf{x}}$ belongs to a target pixel or not.

3. The proposed algorithm

Like the MF, we can find a projection vector $\mathbf{w}=[w_1, \ldots, w_K]^T$ that can separate the target pixels and background pixels by projecting the whitened spectra to $\mathbf{w}$. The MF and the ACE directly use the similarity of $\tilde{\mathbf{d}}$ and $\tilde{\mathbf{x}}$ to detect targets. We can use a new measurement to find the projection vector $\mathbf{w}$. The $\mathbf{w}$ can be found by minimizing $E\{G[(\mathbf{w}-\tilde{\mathbf{d}})^T\tilde{\mathbf{x}}]\}$, where G is a function to measure the difference of the projection of the whitened data $\tilde{\mathbf{x}}$ to $\mathbf{w}$ and $\tilde{\mathbf{d}}$. Since G is a difference measured function, $G(0)$ should be zero; for preventing the bias of negative difference and positive difference between $\tilde{\mathbf{d}}^T\tilde{\mathbf{x}}$ and $\mathbf{w}^T\tilde{\mathbf{x}}$, we require G to be an even function [14]. Generally speaking, G should be functions like quadratic function or quartic function, and should not increase too rapidly to prevent the algorithm is sensitive to outliers [14]. In order to make the algorithm stable, we add the norm constraint $\|\mathbf{w}\|=1$. The constrained minimization problem becomes:

$$\begin{aligned} &\min \Psi(\mathbf{w}) = E\{G[(\mathbf{w}-\tilde{\mathbf{d}})^T\tilde{\mathbf{x}}]\} \\ &s.t.\ \|\mathbf{w}\| = 1 \end{aligned} \tag{5}$$

where G is a difference measured function (such as $G(u)=\log\cosh u$) [14]. After getting the optimal projection vector $\mathbf{w}$, we project the whitened data $\tilde{\mathbf{x}}$ to $\mathbf{w}$, and get the output of DFMF: $y_{DFMF}=\mathbf{w}^T\tilde{\mathbf{x}}$.

If we select the function G as $G(u)=u^2$, the constrained minimization problem becomes:

$$\begin{aligned} &\min \Psi(\mathbf{w}) = E\{[(\mathbf{w}-\tilde{\mathbf{d}})^T\tilde{\mathbf{x}}]^2\} = E\{\mathbf{w}^T\tilde{\mathbf{x}}\tilde{\mathbf{x}}^T\mathbf{w} - 2\mathbf{w}^T\tilde{\mathbf{x}}\tilde{\mathbf{x}}^T\tilde{\mathbf{d}} + \tilde{\mathbf{d}}^T\tilde{\mathbf{x}}\tilde{\mathbf{x}}^T\tilde{\mathbf{d}}\} \\ &= \mathbf{w}^T\boldsymbol{\Gamma}\mathbf{w} - 2\mathbf{w}^T\boldsymbol{\Gamma}\tilde{\mathbf{d}} + \tilde{\mathbf{d}}^T\boldsymbol{\Gamma}\tilde{\mathbf{d}} \\ &s.t.\ \|\mathbf{w}\| = 1 \end{aligned} \tag{6}$$

For the whitened data, $\boldsymbol{\Gamma}=\mathbf{I}$, and we can get the closed form solution:$\mathbf{w}=\tilde{\mathbf{d}}/\|\tilde{\mathbf{d}}\|$. Then, the output of DFMF is:

$$y_{DFMF} = \mathbf{w}^T\tilde{\mathbf{x}} = \frac{\tilde{\mathbf{d}}^T\tilde{\mathbf{x}}}{\|\tilde{\mathbf{d}}\|} \tag{7}$$

Comparing (7) with (3), we can find that $y_{DFMF}=\|\tilde{\mathbf{d}}\|y_{MF}$. For a given hyperspectral image, $\|\tilde{\mathbf{d}}\|$ is a constant, so there is no difference between the detection results of DFMF and MF, when $G(u)=u^2$. Thus, MF can be seen as a special case of DFMF. The only difference between the CEM and the MF is that the CEM uses the correlation matrix, while the MF uses the covariance matrix. If we remove the mean of the hyperspectral image from all pixels, the correlation matrix equals the covariance matrix, and the CEM becomes the MF. Thus, we can also see CEM as a special case of DFMF.

If we select G as $G(u)=\log\cosh u$, we actually measure the sparseness of the difference between $\mathbf{w}^T\tilde{\mathbf{x}}$ and $\tilde{\mathbf{d}}^T\tilde{\mathbf{x}}$. Except the quadratic function, if we select some other difference measured functions, such as $G(u)=\log\cosh u$ and $G(u)=u^4$, there is no closed form solution. In this case, we use the simple gradient descent method [15] to solve the optimization problem. The gradient of $\Psi(\mathbf{w})$ to $\mathbf{w}$ is:

$$\frac{\partial\Psi(\mathbf{w})}{\partial\mathbf{w}} = E\{g[(\mathbf{w}-\tilde{\mathbf{d}})^T\tilde{\mathbf{x}}]\tilde{\mathbf{x}}\} \tag{8}$$

where the function g is the derivative of G.

We have the following gradient descent iterations:

$$\mathbf{w} \leftarrow \mathbf{w} - \mu\frac{\partial\Psi(\mathbf{w})}{\partial\mathbf{w}} \tag{9}$$

$$\mathbf{w} \leftarrow \mathbf{w}/\|\mathbf{w}\| \tag{10}$$

where μ is the learning rate. The difference measured function based matched filter (DFMF) is obtained as follows:

Algorithm outline: DFMF

(1) Center the hyperspectral image data to make the mean zero, and whiten the data to give $\tilde{\mathbf{x}}$. Choose a random initial value for $\mathbf{w}$ such as $\mathbf{w}=[1, 0, 0, \ldots]^T$, and make it norm one. Choose a suitable learning rate μ. In this paper, μ is set to 1.

(2) Update the weight vector by

$$\mathbf{w} \leftarrow \mathbf{w} - \mu E\{g[(\mathbf{w}-\tilde{\mathbf{d}})^T\tilde{\mathbf{x}}]\tilde{\mathbf{x}}\} \tag{11}$$

$$\mathbf{w} \leftarrow \mathbf{w}/\|\mathbf{w}\| \tag{12}$$

(3) Set a convergence criteria: if $\|\mathbf{w}-\mathbf{w}_{old}\|<10^{-4}$, stop. If not converged, go back to step (2).

(4) Project the data $\tilde{\mathbf{x}}$ to $\mathbf{w}$, and get the detection result $\mathbf{w}^T\tilde{\mathbf{x}}$.

The larger the detection result $\mathbf{w}^T\tilde{\mathbf{x}}$ of a pixel is, the more likely the target is present in the pixel. Furthermore, a threshold η can be set, if $\mathbf{w}^T\tilde{\mathbf{x}}>\eta$, we determine the target is present in this pixel; else if $\mathbf{w}^T\tilde{\mathbf{x}}<\eta$, we determine the target is absent in this pixel.

4. Stability of the DFMF

In this section, we proof the stability of the DFMF. The spectrum of the hyperspectral image is assumed to follow the linear spectral mixing model [1,16]: $\hat{\mathbf{x}}=\mathrm{Su}=\sum_{i=1}^{M}\mathbf{s}_i u_i$, where $\hat{\mathbf{x}}$ is the mean removed spectrum. For the linear spectral mixing model, the

spectrum $\hat{\mathbf{x}}$ is assumed to be the linear mixture of M deterministic spectra $\mathbf{s}_1, \ldots, \mathbf{s}_M$ named endmembers, and $u_1, \ldots, u_M$ are the corresponding abundances. Among $\mathbf{s}_1, \ldots, \mathbf{s}_M$ and $u_1, \ldots, u_M$, $\mathbf{s}_k$ and u_k are used to denote the endmember and the abundance of the interesting target, respectively. The whitened spectrum is $\tilde{\mathbf{x}} = \boldsymbol{\Gamma}^{-1/2}\mathrm{Su}$, where $\tilde{\mathbf{x}}$ is the whitened spectrum and $\boldsymbol{\Gamma}$ is the covariance matrix. Denote $\mathbf{A} = \boldsymbol{\Gamma}^{-1/2}\mathbf{S}$, and $\mathbf{a}_1, \ldots, \mathbf{a}_M$ are the columns of the matrix $\mathbf{A}$. Then, we have the following theorem:

Theorem 1. *Assume that spectra of the hyperspectral image follow the linear spectral mixing model and the abundances $u_1, \ldots, u_M$ are independent with each other. Furthermore, suppose the endmember number M is equal to the spectral band number K. Also, assume abundances are independent with each other, $E\{\mathbf{u}\} = \mathbf{0}$, and $E\{\mathbf{u}\mathbf{u}^T\} = \mathbf{I}$. The interesting target's whitened spectral signature $\tilde{\mathbf{d}}$ is assumed to locate in the orthogonal subspace of span$\{\mathbf{a}_l (l = 1, \ldots, M, l \neq k)\}$. Then, with the constraint $\|\mathbf{w}\| = 1$, the local minima of $\Psi(\mathbf{w})$ in (5) include the kth column of the matrix $\mathbf{A}$ if the following inequality holds.*

$$E\{g'(u_k - \tilde{\mathbf{d}}^T\mathbf{a}_k u_k) - u_k g(u_k - \tilde{\mathbf{d}}^T\mathbf{a}_k u_k)\} > 0 \tag{13}$$

where the function g is the derivative of G, and g' is the derivative of g.

Proof. The proof refers to [17–20]. We only prove the case that $k = 1$, the proofs of the other cases ($k \neq 1$) are similar. After the whitening processing, we get:

$$E\{\tilde{\mathbf{x}}\tilde{\mathbf{x}}^T\} = \boldsymbol{\Gamma}^{-1/2}\mathbf{S}E\{\mathrm{uu}^T\}(\boldsymbol{\Gamma}^{-1/2}\mathbf{S})^T = \mathbf{A}E\{\mathrm{uu}^T\}\mathbf{A}^T = \mathbf{I} \tag{14}$$

Under the assumption $E\{\mathbf{u}\mathbf{u}^T\} = \mathbf{I}$, we have $\mathbf{A}\mathbf{A}^T = \mathbf{I}$. Noting that $M = L$, $\mathbf{A}$ is a square matrix. Thus, $\mathbf{A}$ is an orthogonal matrix.

We make the transform $\mathbf{z} = \mathbf{A}^T\mathbf{w}$. Noting that $\mathbf{A}$ is an orthogonal matrix, (5) becomes:

$$\begin{aligned} &\min \Psi_2(\mathbf{z}) = E\{G(\mathbf{z}^T\mathbf{u} - \tilde{\mathbf{d}}^T\mathbf{A}\mathbf{u})\} \\ &s.t. \|\mathbf{z}\| = 1 \end{aligned} \tag{15}$$

The gradient and the Hessian of $\Psi_2(\mathbf{z})$ are:

$$\nabla\Psi_2(\mathbf{z}) = E\{g(\mathbf{z}^T\mathbf{u} - \tilde{\mathbf{d}}^T\mathbf{A}\mathbf{u})\mathbf{u}\} \tag{16}$$

$$\nabla^2\Psi_2(\mathbf{z}) = E\{\mathrm{uu}^T g'(\mathbf{z}^T\mathbf{u} - \tilde{\mathbf{d}}^T\mathbf{A}\mathbf{u})\} \tag{17}$$

$\tilde{\mathbf{d}}$ is assumed to locate in the orthogonal subspace of *span*$\{\mathbf{a}_2, \ldots, \mathbf{a}_M\}$. This assumption is reasonable. Because $\mathbf{a}_2, \ldots, \mathbf{a}_M$ denote these whitened background endmembers, and the assumption means the interesting target's whitened spectral signature $\tilde{\mathbf{d}}$ is orthogonal with the subspace spanned by the whitened background endmembers. Thus, $\tilde{\mathbf{d}}^T\mathbf{A}\mathbf{u} = \tilde{\mathbf{d}}^T\mathbf{a}_1 u_1$. Then (16) and (17) become:

$$\nabla\Psi_2(\mathbf{z}) = E\{g(\mathbf{z}^T\mathbf{u} - \tilde{\mathbf{d}}^T\mathbf{a}_1 u_1)\mathbf{u}\} \tag{18}$$

$$\nabla^2\Psi_2(\mathbf{z}) = E\{\mathrm{uu}^T g'(\mathbf{z}^T\mathbf{u} - \tilde{\mathbf{d}}^T\mathbf{a}_1 u_1)\} \tag{19}$$

We analyze the stability of the point $\mathbf{z} = \mathbf{e}_1$, where $\mathbf{e}_1 = (1, 0, 0, \ldots)^T$. Calculating the gradient and the Hessian at point $\mathbf{z} = \mathbf{e}_1$, and utilizing the independence of the u_i, we obtain:

$$\nabla\Psi_2(\mathbf{e}_1) = \mathbf{e}_1 E\{u_1 g(u_1 - \tilde{\mathbf{d}}^T\mathbf{a}_1 u_1)\} \tag{20}$$

$$\begin{aligned} \nabla^2\Psi_2(\mathbf{e}_1) = &\mathit{diag}\{E[u_1^2 g'(u_1 - \tilde{\mathbf{d}}^T\mathbf{a}_1 u_1)], \\ &E[g'(u_1 - \tilde{\mathbf{d}}^T\mathbf{a}_1 u_1)], E[g'(u_1 - \tilde{\mathbf{d}}^T\mathbf{a}_1 u_1)], \ldots\} \end{aligned} \tag{21}$$

Making a small perturbation $\boldsymbol{\varepsilon}$, we obtain:

$$\begin{aligned} \Psi_2(\mathbf{e}_1 + \boldsymbol{\varepsilon}) &= \Psi_2(\mathbf{e}_1) + \boldsymbol{\varepsilon}^T\nabla\Psi_2(\mathbf{e}_1) + \frac{1}{2}\boldsymbol{\varepsilon}^T\nabla^2\Psi_2(\mathbf{e}_1)\boldsymbol{\varepsilon} + o(\|\boldsymbol{\varepsilon}\|)^2 \\ &= \Psi_2(\mathbf{e}_1) + \varepsilon_1 E\{u_1 g(u_1 - \tilde{\mathbf{d}}^T\mathbf{a}_1 u_1)\} + \frac{1}{2}E\{u_1^2 g'(u_1 - \tilde{\mathbf{d}}^T\mathbf{a}_1 u_1)\}\varepsilon_1^2 \end{aligned}$$

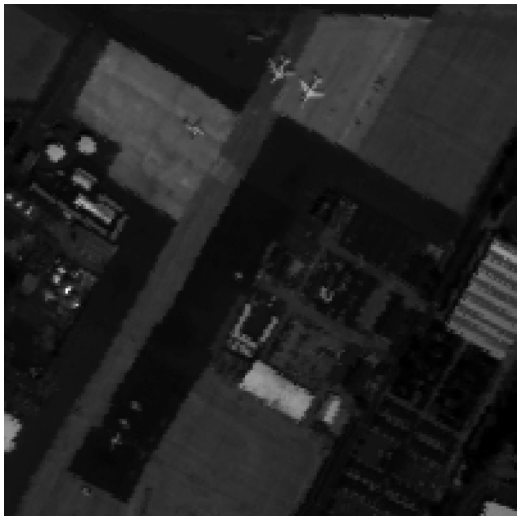

Fig. 1. The first band of the real hyperspectral image.

$$+ \frac{1}{2}E\{g'(u_1 - \tilde{\mathbf{d}}^T\mathbf{a}_1 u_1)\}\sum_{j\neq 1}\varepsilon_j^2 + o(\|\boldsymbol{\varepsilon}\|^2) \tag{22}$$

Because of the constraint $\|\mathbf{z}\| = 1$, we get $\varepsilon_1 = \sqrt{1 - \sum_{j\neq 1}\varepsilon_j^2} - 1$. We notice that $\sqrt{1-\beta} = 1 - \beta/2 + o(\beta)$. Thus, the term of order ε_1^2 in (22) is $o(\|\boldsymbol{\varepsilon}\|^2)$, i.e., of higher order, which can be neglected. We obtain $\varepsilon_1 = -\sum_{j\neq 1}\varepsilon_j^2/2 + o(\|\boldsymbol{\varepsilon}\|^2)$ by using the first-order approximation for ε_1. Finally, we obtain:

$$\begin{aligned} \Psi_2(\mathbf{e}_1 + \boldsymbol{\varepsilon}) = \Psi_2(\mathbf{e}_1) + \frac{1}{2}E\{g'(u_1 - \tilde{\mathbf{d}}^T\mathbf{a}_1 u_1) - u_1 g(u_1 - \tilde{\mathbf{d}}^T\mathbf{a}_1 u_1)\} \\ \times \sum_{j\neq 1}\varepsilon_j^2 + o(\|\boldsymbol{\varepsilon}\|^2) \end{aligned} \tag{23}$$

which proves $\mathbf{z} = \mathbf{e}_1$ or $\mathbf{w} = \mathbf{a}_1$ is a minimum under the conditions of the theorem.

5. Experimental results

In this section, a synthetic hyperspectral image and a real hyperspectral image were used to do experiments. To see how different

Fig. 2. The 20th band of the synthetic hyperspectral image.

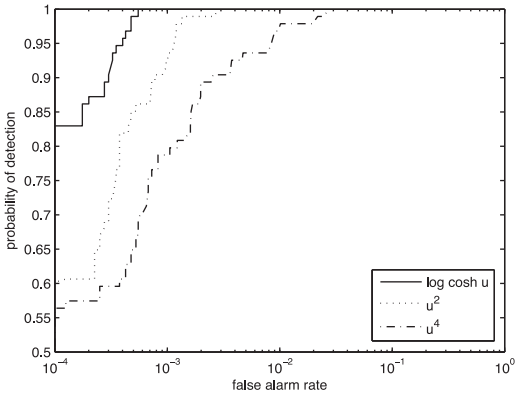

Fig. 3. ROC curves of different difference measured functions for the synthetic hyperspectral image.

functions G in Eq. (5) affect detection results, different functions were chosen, and the results were compared. The proposed algorithm was compared with some other algorithms. We used the receiver operating characteristic (ROC) [1,21] curves to quantitatively evaluate the detection algorithms. The ROC curve plots the detection probabilities vary with the false alarm rates [1,22,23]. A higher ROC curve means the detection algorithm can achieve a higher detection probability under the same false alarm rate, and thus the corresponding algorithm is better.

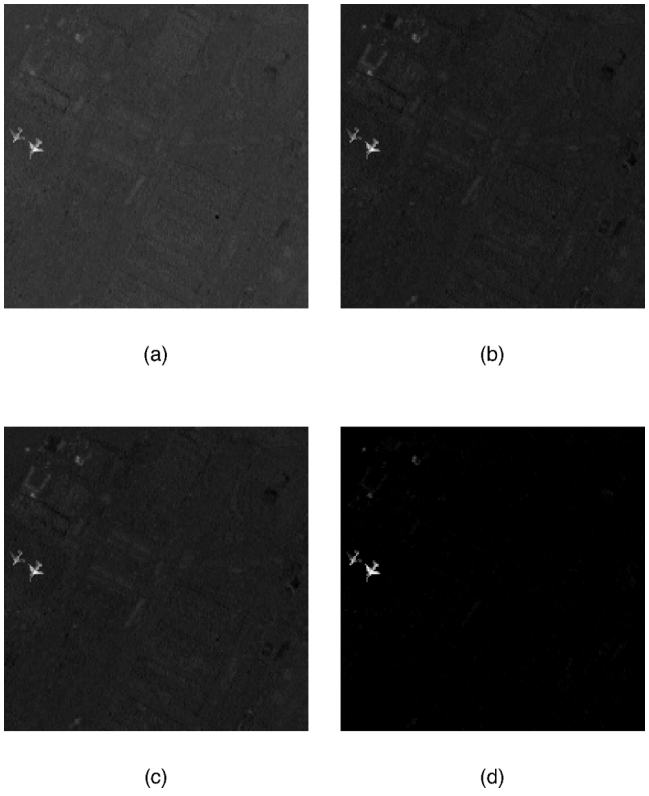

Fig. 4. Detection results of different algorithms for the synthetic hyperspectral image. (a) The detection result of the DFMF for the synthetic hyperspectral image. (b) The detection result of the MF for the synthetic hyperspectral image. (c) The detection result of the CEM for the synthetic hyperspectral image. (d) The detection result of the ACE for the synthetic hyperspectral image.

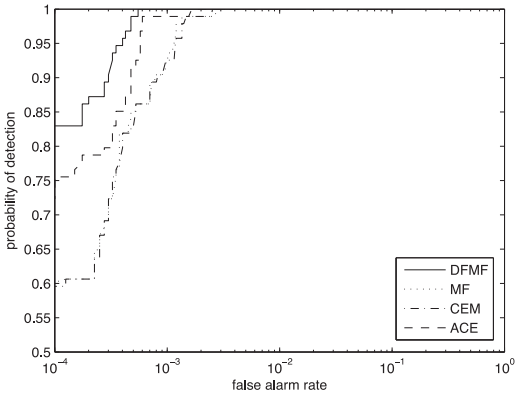

Fig. 5. ROC curves of different algorithms for the synthetic hyperspectral image.

5.1. Synthetic hyperspectral image experiments

We used the real hyperspectral image collected by the Airborne Visible/Infrared Imaging Spectrometer (AVIRIS) sensor to design a synthetic hyperspectral image. Fig. 1 shows the first band of the real hyperspectral image. The scene is a part of the San Diego airport. The AVIRIS collected data in 224 bands, and the spectral coverage was from 0.4 μm to 2.5 μm [2]. After removing water absorption and low *SNR* bands, we had 189 bands left. There are three airplanes in the real hyperspectral image as shown in Fig. 1. We removed two of the three airplanes and implanted the two removed airplanes to another part of the San Diego airport to design a synthetic hyperspectral image with 200×200 pixels. Fig. 2 shows the 20th band of the synthetic hyperspectral image.

To see how different difference measured functions affect the detection results of the proposed algorithm DFMF, we chose three different functions: $G(u) = u^2$, $G(u) = u^4$ and $G(u) = \log\cosh u$ to do experiments. Fig. 3 shows the ROC curves of these three functions. From Fig. 3, we can see $G(u) = \log\cosh u$ performs best. We compared the DFMF with the MF, the CEM, and the ACE. Since $G(u) = \log\cosh u$ had the best detection result among the three experimental difference measured functions, $G(u) = \log\cosh u$ was used in the DFMF. Figs. 4 and 5 show the detection results and ROC curves of different algorithms, respectively. In Fig. 5, ROC curves of the MF and the CEM are almost overlapped. From Figs. 4 and 5, we can see the performance of the DFMF is best.

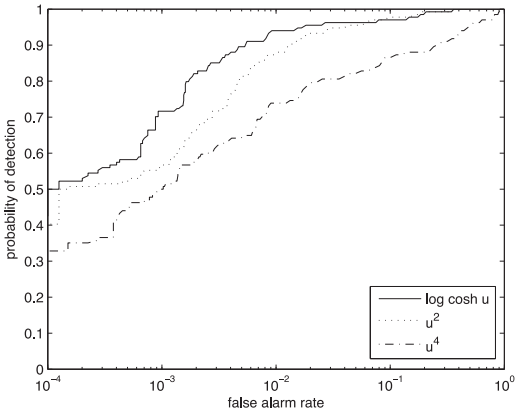

Fig. 6. ROC curves of different difference measured functions for the real hyperspectral image.

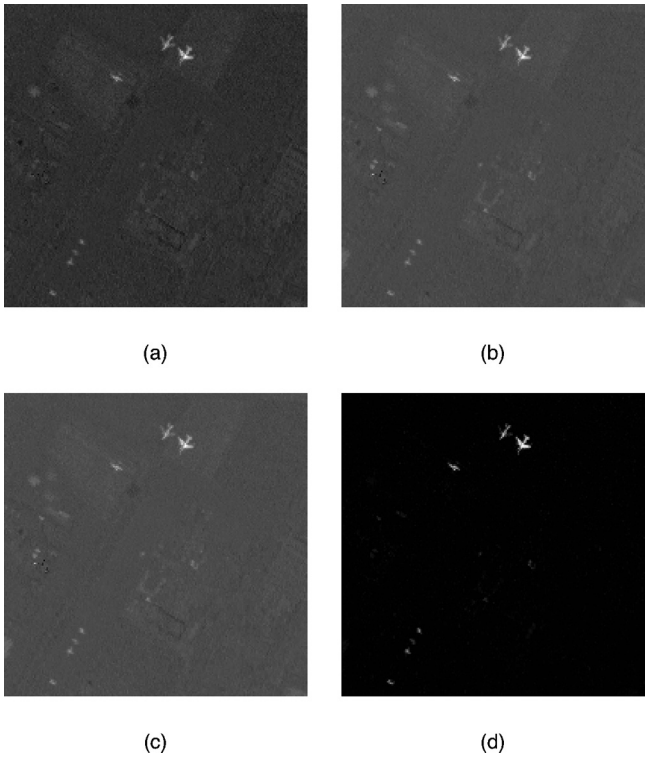

Fig. 7. Detection results of different algorithms for the real hyperspectral image. (a) The detection result of the DFMF for the real hyperspectral image. (b) The detection result of the MF for the real hyperspectral image. (c) The detection result of the CEM for the real hyperspectral image. (d) The detection result of the ACE for the real hyperspectral image.

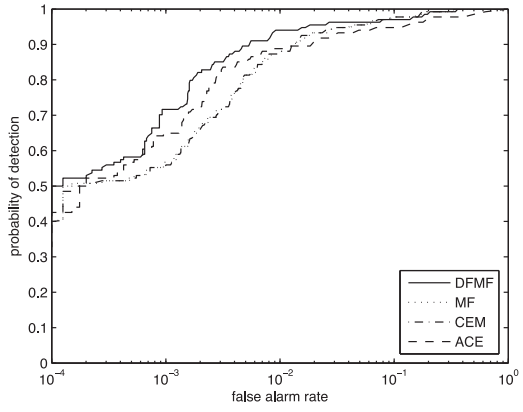

Fig. 8. ROC curves of different algorithms for the real hyperspectral image.

5.2. Real hyperspectral image experiments

In this section, we used the Fig. 1 shown real hyperspectral image to conduct experiments. We also chose the three functions: $G(u) = u^2$, $G(u) = u^4$ and $G(u) = \log\cosh u$ for the DFMF. Fig. 6 shows the ROC curves of these three functions. Once again, the performance of $G(u) = \log\cosh u$ is best. The DFMF was compared to the MF, the CEM, and the ACE. $G(u) = \log\cosh u$ was used in the DFMF. The Detection results and ROC curves of different algorithms are shown in Figs. 7 and 8, respectively. ROC curves of the MF and the CEM are almost overlapped in Fig. 8. Figs. 7 and 8 indicate the DFMF behaves best. The experimental results demonstrate for the real hyperspectral image, the DFMF performs better.

6. Conclusion

A new target detection algorithm for the hyperspectral image is proposed in this paper. The algorithm uses a difference measured function to build an objective function, and transforms the target detection to a constrained optimization problem. The gradient descent method is utilized to solve the constrained optimization problem. We also find the proposed algorithm could include the MF as a special case. One synthetic hyperspectral image and one real hyperspectral image were used to do experiments. The experimental results show the proposed algorithm behaves better than the other experimental algorithms. Performances of different difference measured functions were also compared, and the results show the $G(u) = \log\cosh u$ is a good choice.

References

[1] D. Manolakis, D. Marden, G.A. Shaw, Hyperspectral image processing for automatic target detection applications, Lincoln Lab. J. 14 (1) (2003) 79–116.
[2] G.A. Shaw, H.K. Burke, Spectral imaging for remote sensing, Lincoln Lab. J. 14 (1) (2003) 3–28.
[3] D. Manolakis, G. Shaw, Detection algorithms for hyperspectral imaging applications, IEEE Signal Process. Mag. 19 (1) (2002) 29–43.
[4] S.M. Kay, Fundamentals of Statistical Signal Processing, Prentice Hall, Englewood Cliffs, NJ, 1998.
[5] D.G. Manolakis, V.K. Ingle, S.M. Kogon, Statistical and Adaptive Signal Processing: Spectral Estimation, Signal Modeling, Adaptive Filtering and Array Processing, McGraw-Hill, Boston, 2000.
[6] E. Conte, M. Lops, G. Ricci, Asymptotically optimum radar detection in compound-Gaussian clutter, IEEE Trans. Aerosp. Electron. Syst. 31 (2) (1995) 617–625.
[7] L.L. Scharf, L.T. McWhorter, Adaptive matched subspace detectors and adaptive coherence estimators, in: Proceedings of the 1996 30th Asilomar Conference on Signals, Systems and Computers, Pacific Grove, CA, USA, 1996.
[8] S. Kraut, L.L. Scharf, The CFAR adaptive subspace detector is a scale-invariant GLRT, IEEE Trans. Signal Process. 47 (9) (1999) 2538–2541.
[9] S. Kraut, L.L. Scharf, L.T. McWhorter, Adaptive subspace detectors, IEEE Trans. Signal Process. 49 (1) (2001) 1–16.
[10] A. Hyvärinen, E. Oja, Independent component analysis: algorithms and applications, Neural Netw. 13 (4-5) (2000) 411–430.
[11] J.C. Harsanyi, Detection and classification of subpixel spectral signatures in hyperspectral image sequences, Ph.D. dissertation, Department of Electrical Engineering, University of Maryland Baltimore County, 1993.
[12] W.H. Farrand, J.C. Harsanyi, Mapping the distribution of mine tailings in the Coeur d'Alene River valley, Idaho, through the use of a constrained energy minimization technique, Remote Sens. Environ. 59 (1) (1997) 64–76.
[13] C.-I. Chang, Hyperspectral Imaging: Techniques for Spectral Detection and Classification, Kluwer Academic/Plenum Publishers, New York, 2003.
[14] E. Oja, L. Wang, Robust fitting by nonlinear neural units, Neural Netw. 9 (3) (1996) 435–444.
[15] J. Nocedal, S.J. Wright, Numerical Optimization, Springer, New York, 2000.
[16] J.B. Adams, M.O. Smith, A.R. Gillespie, Imaging Spectroscopy: Interpretation Based on Spectral Mixture Analysis, Cambridge University Press, Cambridge, 1993.
[17] A. Hyvärinen, E. Oja, Independent component analysis by general nonlinear Hebbian-like learning rules, Signal Process. 64 (1998) 301–313.
[18] Z. Shi, C. Zhang, Semi-blind source extraction for fetal electrocardiogram extraction by combining non-Gaussianity and time-correlation, Neurocomputing 70 (7-9) (2007) 1574–1581.
[19] Z. Shi, C. Zhang, Blind source extraction using generalized autocorrelations, IEEE Trans. Neural Netw. 18 (5) (2007) 1516–1524.
[20] H. Zhang, Z. Shi, C. Guo, Blind source extraction based on generalized autocorrelations and complexity pursuit, Neurocomputing 72 (10-12) (2009) 2556–2562.
[21] T. Fawcett, An introduction to ROC analysis, Pattern Recogn. Lett. 27 (8) (2006) 861–874.
[22] D. Manolakis, R. Lockwood, T. Cooley, J. Jacobson, Is there a best hyperspectral detection algorithm? in: Proc. SPIE, Orlando, USA, 2009.
[23] Y. Gu, Y. Liu, Y. Zhang, A selective KPCA algorithm based on high-order statistics for anomaly detection in hyperspectral imagery IEEE Geosci. Remote Sens. Lett. 5 (1) (2008) 43–47.